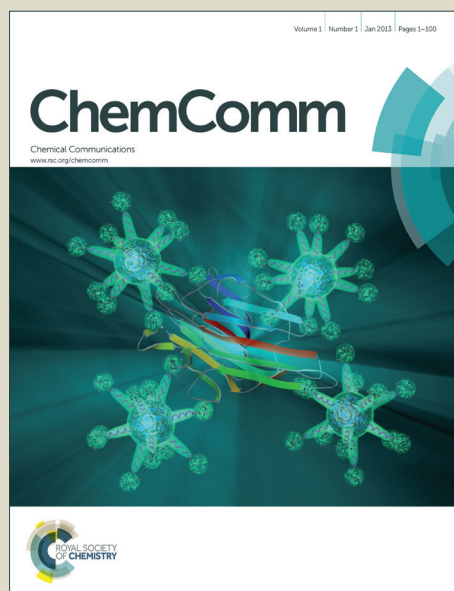


ChemComm

Accepted Manuscript



This is an *Accepted Manuscript*, which has been through the Royal Society of Chemistry peer review process and has been accepted for publication.

Accepted Manuscripts are published online shortly after acceptance, before technical editing, formatting and proof reading. Using this free service, authors can make their results available to the community, in citable form, before we publish the edited article. We will replace this *Accepted Manuscript* with the edited and formatted *Advance Article* as soon as it is available.

You can find more information about *Accepted Manuscripts* in the [Information for Authors](#).

Please note that technical editing may introduce minor changes to the text and/or graphics, which may alter content. The journal's standard [Terms & Conditions](#) and the [Ethical guidelines](#) still apply. In no event shall the Royal Society of Chemistry be held responsible for any errors or omissions in this *Accepted Manuscript* or any consequences arising from the use of any information it contains.

COMMUNICATION

Comparative STM study of mixed ligand monolayers on gold nanoparticles in air and in 1-phenyloctane

Cite this: DOI: 10.1039/x0xx00000x

Quy Khac Ong,^a Shun Zhao,^a Javier Reguera,^a Fabio Biscarini,^b and Francesco Stellacci^a

Received 00th January 2012,

Accepted 00th January 2012

DOI: 10.1039/x0xx00000x

www.rsc.org/

Scanning tunnelling microscopy (STM) studies have found stripe-like domains on gold nanoparticles (NPs) coated with certain binary mixtures of ligand molecules. The majority of these NPs' properties have been investigated for particles in solvents. Yet, most STM studies are for NPs in a dry state. Images of the same particles in air and liquid had not been obtained yet. In this work, a judicious choice of ligands molecules led to NPs with close-to-ideal STM imaging condition in air and in 1-phenyloctane (PO). Large datasets in both conditions were acquired and rapidly evaluated through power spectral density (PSD) analysis. The result is a quantitative comparison of stripe-like domains in air and PO on the same NPs. PSD analysis determines a characteristic length-scale for these domains of ~1.0 nm in air and in PO showing persistence of striped domains in these two media. A length scale of ~0.7 nm for homoligand NPs was found.

It has been shown that when binary mixtures of thiolated ligands co-assemble onto gold flat surfaces, phase-separation occurs and domains of each molecule form within the self-assembled monolayer (SAM).¹ This is expected when surface mobility of the ligands is present. SAMs of thiolated molecules have been used as ligand shell for gold NPs.² The ligand shell imparts several properties, from solubility to bio-functionality.³ Thiolated ligands on gold NPs have mobility either larger or comparable to that on flat SAMs.⁴ Certain binary mixtures of ligand molecules on gold NPs separate into domains as they do on flat surfaces. Binary mixtures of thiols spontaneously form stripe-like domains with a width of ~1 nm. These domains have been characterized by STM and atomic force microscopy (AFM).⁵ The existence of stripe-like domains has been confirmed by three independent laboratories.⁶ All of the images obtained were analysed by a power spectral density (PSD) analysis that readily extracts both NP and molecular domain sizes from a whole image rapidly.^{6a} Phase separation in the ligand shell into small domains has been confirmed by a series of other spectroscopic

techniques.⁷ Simulations developed in Glotzer's group have shown the existence of these domains on NPs.⁸ Many structure-dependent properties have been shown for striped NPs, e.g. non-monotonic dependence of interfacial energy^{5b} and of solubility limit⁹ on the ligand shell composition, specific interaction with cell-membranes;¹⁰ or selective complexation of ions.¹¹

These properties have been established in liquids; but most of the scanning probe images are in air or in vacuum. Images of striped NPs in liquids have been obtained in atomic force microscopy and STM but only for particles that could not be readily imaged in air. To date, there has not been a direct comparison of images of the same sample in air and in liquid. Herein, we show the first of such studies in which large data sets of images of NPs in air and PO are analysed. The chosen mixed ligand monolayers of NPs are composed of a mixture of 1-nonanethiol (NT) and 4-methylbenzenethiol (MBT). To approach the challenge of imaging simultaneously in air and PO, we chose a couple of ligands (NT and MBT) that had consistently given good STM contrast and that are hydrophobic to optimize the wetting in the apolar solvent we use for STM imaging (PO). We synthesized a series of NT:MBT NPs with various ligand shell compositions, but only one composition (1:2 NT:MBT) could be imaged consistently in both air and liquid with similar contrast. The NPs were synthesized according to a modified Stucky method¹² and characterized as detailed in ESI. For the two NPs studied here NP1 were coated with 1-octanethiol, and NP2 with a 1:2 (reaction stoichiometry) mixture of NT and MBT. The ligand shell density (4.9 and 5.8 ligands/nm² for NP1 and NP2 respectively) was found higher than that for flat surfaces (4.6 ligands/nm²) coated either with aliphatic or aromatic thiolated molecules.¹³ This increase is consistent with what has been previously reported.¹³ STM samples were prepared via Langmuir films that were transferred onto functionalized Au(111)-coated mica substrates using Langmuir-Schaefer deposition. STM images were obtained from a Bruker Multimode Nanoscope IIIA equipped with an E-scanner. Current setpoints were typically set in the range from 40 to 500 pA, bias voltage from 100 mV-1200 mV, integral gain from 0.4-0.5, and proportional gain from 0.7-1.0.

The first sets of images that were acquired on these samples were recorded in air. When NP2 was first imaged, it was immediately clear that the ligand molecules were chosen correctly, as images of clear stripe-like domains with good contrast were readily achievable. It was possible to obtain good images of the NPs with visible stripe-like domains from a scan size of 10 nm to a scan size of ~50 nm. The horizontal PSD plots for this images were substantially identical to what was described recently by Biscarini et al.^{6a} Fig. 1 shows a series of images taken at different scan angles, scan sizes, and tip

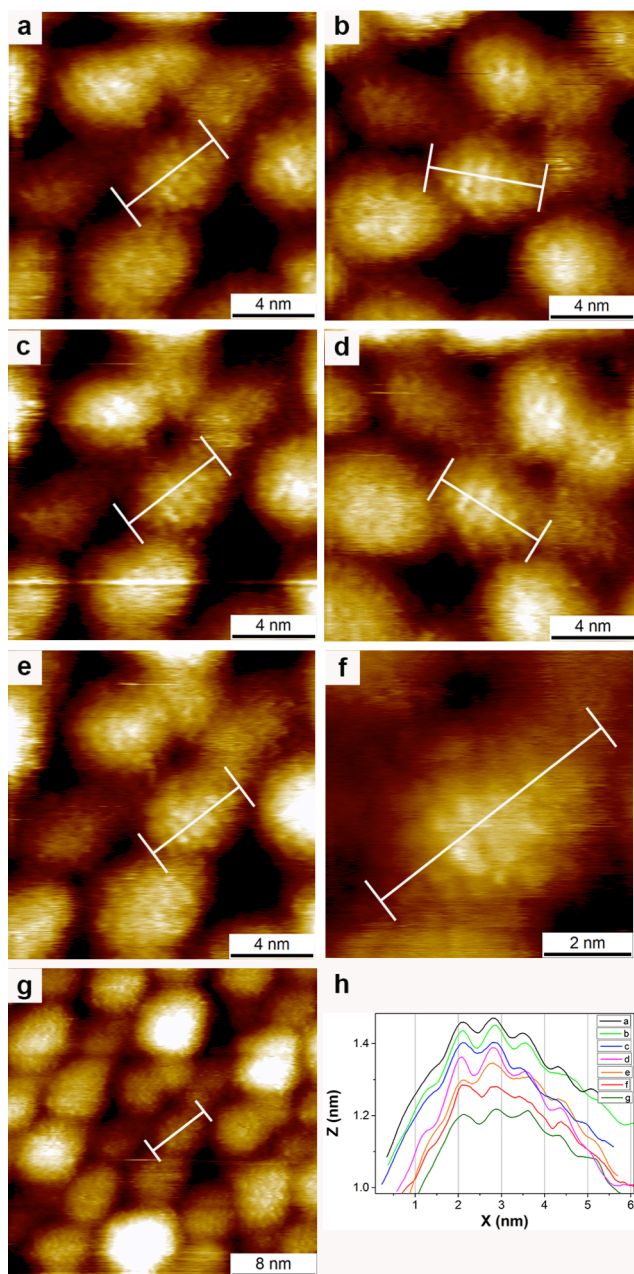


Figure 1. STM topography images of NP2 recorded in air at different scanning angles and scan sizes. All images are original trace scans of 512x512 pixels. (a) scanning angle = 0°, (b) 310°, (c) 0°, (d) 290°, (e,f,g) 0°. (h) Cross section lines going across the same particles on each image to show the remarkable consistency of the features on the NPs. The lines on each image (a-g) are the exact cross sections used and their ends indicate average width. Full image data sets for all of the images shown in this figure can be found in ESI.

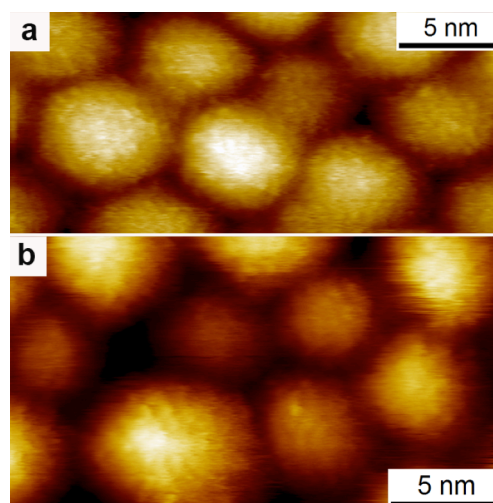


Figure 2. STM topography images of NP1 in air (a) and NP2 in PO (b). Full image data sets can be found in ESI.

velocities. The persistence of the image cross sections performed on the same particle (Fig. 1h) points out to a remarkable stability for the feature on the particle studied across many images. We should point out that these features are not fixed or immobile, as the ligands have a certain degree of mobility. However, the cross sections shown, calculated over a ~2 nm width, indicate an average feature size that is conserved within the time of the experiment.

In order to compare the images of NP2 to those of control NPs, we imaged homoligand NPs (NP1). As done in the past,^{5a} these NPs were used to establish the molecular nature of the feature observed on the particles as well as the validity of our method to establish the characteristic length scales associated with these features. NP1 were imaged only in air (Fig. 2a) because in PO most samples showed relatively rapid desorption from the substrate due to their solubility. NP2 was also imaged in PO. PO is a relatively poor solvent for these NPs (UV-Vis in Fig. S3, ESI). The choice of PO was dictated by the fact that it is a common STM solvent providing clean imaging conditions by avoiding accumulation of moisture on the surface while not disturbing image acquisition due to its low volatility.¹⁴ Images obtained in PO showed stripe-like domains (Fig. 2b) as the ones observed in air. Image cross-sectional analysis confirms this observation. Images of NPs in PO were taken at different scan sizes and tip speeds (Fig. S7c, f). In all cases the features on the NPs are invariant to imaging parameters. We show that the features remain when higher magnification images are acquired (Fig. S7). We also show (both via line profiles and PSD plots) that images acquired with all other imaging parameters kept constant but varying solely tip speed or integral gains show invariance of the imaged features (Fig. S8 and S9, ESI). Herein, we can comment on the role of gains in our images. We set integral gains in a limited range upon a series of considerations among which the ability to track NP surfaces by an STM tip. The integral-gain range was chosen to be sufficiently small to avoid feedback loop artifacts while allowing the tip to follow the curvature of the NPs and more importantly to reveal molecular features. The gain settings dictate contrast and sharpness of STM images. The importance of gain setting is illustrated in Fig. S10, ESI, where the integral gain was varied while imaging an HOPG sample. At lower gain setting, carbon atoms of the surface layer are imaged giving discrete circular features on the image, but when the gain is raised sufficiently high the features smear into rows of high contrast. Despite the high gain, the characteristic spacing of graphite is still maintained. Hence, all of the controls performed indicate that the features we observe are due to true tip-sample interaction.

All the images shown in Figures 1 and 2 show domains on the NPs. Cross sections of the images indicate a certain variation in characteristic spacing; analysis of a large data set can better establish quantitative similarities and differences between images. We could for example discuss the case of **NP1**. Images such as Fig. 2a show domains that could -in some places- be described as stripe-like domains. These domains are derived from the imaging of groups of ligands whose image blurs into stripes, exactly as illustrated in the image of graphite at higher gains (Fig. S10, ESI). The same phenomenon happens for mixed ligand **NP2** where ligands of the same chemical nature can be individually imaged but as the resolution lowers their features merge into stripe-like domains as shown in Fig. 2b of ref. [6b]. The characteristic difference between homoligand and mixed ligand NPs is that the former show a spacing of ~ 0.5 nm and the latter a spacing of ~ 1 nm. Recently, stripe-like domains with a ~ 0.6 nm spacing on homoligand NPs have been imaged.¹⁵ We have described this type of images in the past.^{5a} At higher resolution single molecule images (dots) with a ~ 0.5 nm spacing have been imaged by us and by others.¹⁶ In this paper, to extract the characteristic spacing of the domains present on the NPs we resorted to two methods. We analysed image cross-sections and fitted the average PSD plots. The first method allows for an operator to find the direction of minimum distance between neighbouring domains as illustrated in Fig. 1. The operator then records the distance read directly on the cross section. The drawback of this approach is that it is -in principle- subjective. To mitigate it, two operators carried out the measurements presented here, independently. The second approach starts by analysing the PSD plot, where the shoulder/peak between $k \sim 3 \times 10^9 \text{ m}^{-1}$ and $k \sim 10 \times 10^9 \text{ m}^{-1}$ region (in blue in Fig. 3a) indicates the presence of features on NPs with a characteristic correlation length in the nm scale. The more the 'peak'/inflection (red dot) in the blue region moves to the right the smaller the characteristic dimension of the features. The extraction of this characteristic length is done by fitting the plots with a functional that was developed and tested in ref. [6a]. We fit the average curves and extracted the parameter associated with the characteristic length-scale of the domains present on the particles. The fits and parameters are displayed in Fig. S15 and Table S2.16, ESI. We decided to adopt both methods as their validity is mutually strengthened by the fact that the results are virtually identical.

In Fig. 3b and 3c we show PSD plots for all of the good images achieved for our samples. Images were chosen based on the presence of molecular features on the NPs without any other evaluation. The variation in quality of the images in terms of crispness of the features is caused by the tip and its changes in the optimal scanning parameters during the measurements. It is immediately evident that the PSDs of these large datasets show a remarkable consistency with all the PSD plots having the same shape. All the PSD plots achieved from images of **NP1** and **NP2** (in air) are shown in Fig. 3b. A clear shift of the shoulder associated with feature on nanoparticles towards lower spacing (to the right) of the **NP1** PSD plots (blue) relative to the same shoulder for **NP2** PSD plots (red) is observed. In Fig. 3c we show all the PSD plots for **NP2** in air and in PO. There is an obvious overlap between these two groups of PSD plots, indicating a lack of significant differences for the images obtained in these two environments. To further compare all of the sets of curves shown we decided to produce average PSD plots from the images having a 30 nm scan size (the most common in our data sets). Fig. S12-14, ESI, show that these average plots all fall in the middle of all of the PSD plots. The comparison of the average plots confirms the conclusions achieved by inspecting the sets of PSDs visually. **NP2** in air shows domains spaced $0.89 \text{ nm} \pm 0.17 \text{ nm}$ when measured via cross-section analysis and 1.04 nm from the fit. The same NPs in PO

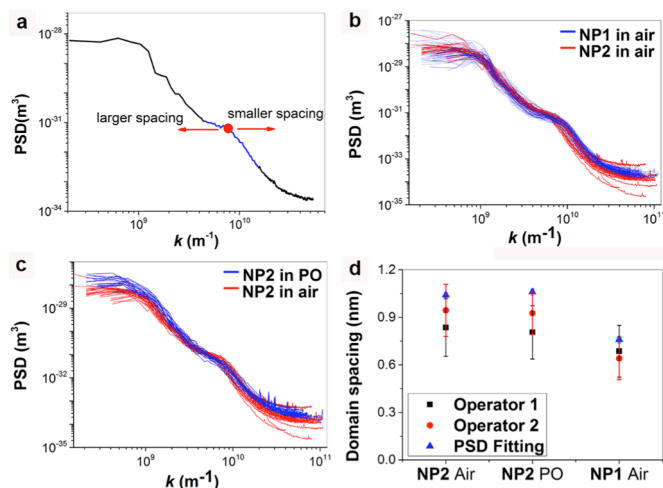


Figure 3. PSD plots for all of the images analysed in this paper. a) a typical PSD plot of an STM image; the blue segment is the characteristic ligand spacing. The deflection point marked by the red dot is a good indicator of the characteristic spacing. Its shift to a smaller or larger value is indicated by the direction of red arrows. Comparison for the plots: (b) of **NP1** (blue) and **NP2** (red) in air and (c) of **NP2** in PO (blue) and air (red). (d) Characteristic length scales of all the samples obtained from direct measurements on trace images and PSD fits. The manual measurements were performed via NP cross-section profiles by two independent operators. Error bars are \pm one standard deviation.

show spacings of $0.86 \text{ nm} \pm 0.15 \text{ nm}$ (cross section) and 1.06 nm from the fit. As a reference, the measurements for homoligand NPs are of $0.66 \text{ nm} \pm 0.15 \text{ nm}$ (cross section) and 0.76 nm (from PSD fitting). We believe that the values extracted from PSD fitting are somewhat larger than the manual measurements because they only report distances in the horizontal direction and they take in account the whole images, hence weighing in also defects. Importantly no matter what the measuring approach is we can affirm that homoligand particles have a domain distance of ~ 0.7 nm and **NP2** particles have a domain width of ~ 1.0 nm independent of the imaging media. We should point out all of the images presented here were recorded with the STM operator not knowing which sample he was imaging.

Conclusions

We have shown comparative studies of mixed ligand NPs imaged with STM in air and in a solvent (PO). Image analysis determines that these NPs present stripe-like domains in both cases. These domains are qualitatively very similar and have a characteristic spacing of ~ 1.0 nm independent of the imaging media.

This work was supported by the Swiss National Science Foundation.

Notes and references

^a Institute of Materials, EPFL, Switzerland.

^b Dip. Scienze della Vita, Università di Modena e Reggio Emilia, Via Campi 183, 41125 Modena, Italy.

Electronic Supplementary Information (ESI) available: Nanoparticle synthesis, NMR characterization, TEM and TGA analysis, STM images, and PSD fitting results. See DOI: 10.1039/c000000x/

- ¹ (a) A. V. Shevade, J. Zhou, M. T. Zin and S. Jiang, *Langmuir*, 2001, **17**, 7566; (b) S. J. Stranick, S. V. Atre, A. N. Parikh, M. C. Wood, D. L. Allara, N. Winograd and P. S. Weiss, *Nanotechnology*, 1996, **7**, 438; (c) S. J. Stranick, M. M. Kamna, K. R. Krom, A. N. Parikh, D. L. Allara and P. S. Weiss, *J. Vac. Sci. Technol., B*, 1994, **12**, 2004; (d) S. J. Stranick, A. N. Parikh, Y. T. Tao, D. L. Allara and P. S. Weiss, *J. Phys. Chem.*, 1994, **98**, 7636; (e) H. I. Kim, T. Koini, T. R. Lee and S. S. Perry, *Langmuir*, 1997, **13**, 7192.
- ² (a) M.-C. Daniel and D. Astruc, *Chem. Rev.*, 2003, **104**, 293; (b) M. Brust, M. Walker, D. Bethell, D. J. Schiffrin and R. Whyman, *Chem. Commun.*, 1994, 801; (c) M. Brust, J. Fink, D. Bethell, D. J. Schiffrin and C. Kiely, *Chem. Commun.*, 1995, 1655; (d) R. H. Terrill, T. A. Postlethwaite, C.-h. Chen, C.-D. Poon, A. Terzis, A. Chen, J. E. Hutchison, M. R. Clark and G. Wignall, *J. Am. Chem. Soc.*, 1995, **117**, 12537; (e) A. C. Templeton, W. P. Wuelfing and R. W. Murray, *Acc. Chem. Res.*, 2000, **33**, 27.
- ³ (a) R. Sardar, A. M. Funston, P. Mulvaney and R. W. Murray, *Langmuir*, 2009, **25**, 13840; (b) M. De, P. S. Ghosh and V. M. Rotello, *Adv. Mater.*, 2008, **20**, 4225.
- ⁴ (a) S. Rapino and F. Zerbetto, *Small*, 2007, **3**, 386; (b) P. Ionita, A. Volkov, G. Jeschke and V. Chechik, *Anal. Chem.*, 2007, **80**, 95; (c) A. Caragheorghopol and V. Chechik, *PCCP*, 2008, **10**, 5029.
- ⁵ (a) A. M. Jackson, Y. Hu, a. Paulo Jacob Silva and F. Stellacci, *J. Am. Chem. Soc.*, 2006, **128**, 11135; (b) J. J. Kuna, K. Voitchovsky, C. Singh, H. Jiang, S. Mwenifumbo, P. K. Ghorai, M. M. Stevens, S. C. Glotzer and F. Stellacci, *Nat. Mater.*, 2009, **8**, 837.
- ⁶ (a) F. Biscarini, Q. K. Ong, C. Albonetti, F. Liscio, M. Longobardi, K. S. Mali, A. Ciesielski, J. Reguera, C. Renner, S. De Feyter, P. Samori and F. Stellacci, *Langmuir*, 2013, **29**, 13723; (b) Q. K. Ong, J. Reguera, P. J. Silva, M. Moglianetti, K. Harkness, M. Longobardi, K. S. Mali, C. Renner, S. De Feyter and F. Stellacci, *ACS Nano*, 2013, **7**, 8529.
- ⁷ (a) A. Centrone, Y. Hu, A. M. Jackson, G. Zerbi and F. Stellacci, *Small*, 2007, **3**, 814; (b) X. Liu, M. Yu, H. Kim, M. Marnett and F. Stellacci, *Nat. Commun.*, 2012, **3**, 1182; (c) M. Moglianetti, Q. K. Ong, J. Reguera, K. M. Harkness, M. Marnett, A. Radulescu, J. Kohlbrecher, C. Jud, D. I. Svergun and F. Stellacci, *Chem. Sci.*, 2014, **5**, 1232.
- ⁸ (a) C. Singh, P. Ghorai, M. Horsch, A. Jackson, R. Larson, F. Stellacci and S. Glotzer, *Phys. Rev. Lett.*, 2007, **99**, 226106; (b) S. C. Glotzer and M. J. Solomon, *Nat. Mater.*, 2007, **6**, 557; (c) P. K. Ghorai and S. C. Glotzer, *J. Phys. Chem. C*, 2010, **114**, 19182; (d) A. Santos, J. A. Millan and S. C. Glotzer, *Nanoscale*, 2012, **4**, 2640.
- ⁹ A. Centrone, E. Penzo, M. Sharma, J. W. Myerson, A. M. Jackson, N. Marzari and F. Stellacci, *Proc. Natl. Acad. Sci. U. S. A.*, 2008, **105**, 9886.
- ¹⁰ A. Verma, O. Uzun, Y. Hu, Y. Hu, H.-S. Han, N. Watson, S. Chen, D. J. Irvine and F. Stellacci, *Nat. Mater.*, 2008, **7**, 588.
- ¹¹ E. S. Cho, J. Kim, B. Tejerina, T. M. Hermans, H. Jiang, H. Nakanishi, M. Yu, A. Z. Patashinski, S. C. Glotzer, F. Stellacci and B. A. Grzybowski, *Nat. Mater.*, 2012, **11**, 978.
- ¹² N. Zheng, J. Fan and G. D. Stucky, *J. Am. Chem. Soc.*, 2006, **128**, 6550.
- ¹³ (a) M. J. Hostetler, J. E. Wingate, C.-J. Zhong, J. E. Harris, R. W. Vachet, M. R. Clark, J. D. Londono, S. J. Green, J. J. Stokes, G. D. Wignall, G. L. Glish, M. D. Porter, N. D. Evans and R. W. Murray, *Langmuir*, 1998, **14**, 17; (b) K. Seo and E. Borguet, *J. Phys. Chem. C*, 2007, **111**, 6335; (c) D. G. Matei, H. Muzik, A. Götzhäuser and A. Turchanin, *Langmuir*, 2012, **28**, 13905; (d) Q. Jin, J. A. Rodriguez, C. Z. Li, Y. Darici and N. J. Tao, *Surf. Sci.*, 1999, **425**, 101.
- ¹⁴ (a) S. De Feyter and F. C. De Schryver, *J. Phys. Chem. B*, 2005, **109**, 4290; (b) W. Mamdouh, H. Uji-i, J. S. Ladislaw, A. E. Dulcey, V. Percec, F. C. De Schryver and S. De Feyter, *J. Am. Chem. Soc.*, 2005, **128**, 317; (c) K. S. Mali, J. Adisoejoso, E. Ghijssens, I. De Cat and S. De Feyter, *Acc. Chem. Res.*, 2012, **45**, 1309.
- ¹⁵ M. A. Mezour, I. I. Perepichka, J. Zhu, R. B. Lennox and D. F. Perepichka, *ACS Nano*, 2014, **8**, 2214.
- ¹⁶ (a) M. Yu and F. Stellacci, *Small*, 2012, **8**, 3720; (b) K. V. Sarathy, G. Raina, R. T. Yadav, G. U. Kulkarni and C. N. R. Rao, *J. Phys. Chem. B*, 1997, **101**, 9876.